Physical parameters characterizing dysfunction of neuronal cargo transport caused by the dynein inhibitor ciliobrevin

Kumiko Hayashi[1,*], Miki G. Miyamoto[1], and Shinsuke Niwa[2]

[1]Department of Applied Physics, Graduate School of Engineering, Tohoku University, Sendai, Japan

[2]Frontier Research Institute for Interdisciplinary Sciences and Graduate School of Life Science, Tohoku University, Sendai, Japan

*** Correspondence.**

E-mail: kumiko@camp.apph.tohoku.ac.jp (K.H.)

Abstract

Synaptic cargo transport by the motor proteins kinesin and dynein in the axons of hippocampal neurons was investigated using non-invasive measurement of transport force based on non-equilibrium statistical mechanics and extreme-value statistics on the maximum transport velocity. Although direct physical measurements such as force measurement using optical tweezers are difficult in a non-equilibrium intracellular environment, the proposed non-invasive estimations enabled enumerating force producing units (FPUs) carrying a cargo comprising the motor proteins generating force. The number of FPUs served as a barometer for the stable and long-distance transport by multiple motors, which was then used to quantify the extent of damage to axonal transport resulting from ciliobrevin, a dynein inhibitor. Our results show interrelationships among force, velocity, and the number of FPUs, precisely describing transport dysregulation. Such measures may help quantify the damage to axonal transport resulting from neuronal diseases including Alzheimer's, Parkinson's, and Huntington's diseases in future.

Introduction

A neuron includes a long process called an axon that connects the cell body to the terminal. Synaptic proteins are produced and packed as cargo vesicles in the cell body of neurons, after which the cargos are transported in an anterograde manner to the terminal through the axon by KIF1A and KIF1Bβ, members of the kinesin-3 family, and in a retrograde manner by cytoplasmic dynein, producing driving force hydrolyzing adenosine triphosphate (ATP) molecules[1, 2, 3]. Elucidation of the physical aspects of the synaptic cargo transport mechanism can potentially lead to quantitative understanding the process of synapse creation at the terminal region of neurons, and deficits of which are often related to neuronal diseases, such as Alzheimer's, Parkinson's, and Huntington's diseases[4, 5]. Considering the difficulties associated with direct physical measurements in non-equilibrium living neurons, our aim was to non-invasively estimate information concerning the physical parameters of axonal transport by using knowledge of non-equilibrium statistical mechanics developed for the transport of non-living materials, such as thermal conduction and electrical conduction.

Results

Fluctuation properties for CVSs of moving cargos

The motion of synaptic cargos along the axon of mice hippocampal neurons was observed by fluorescence microscopy (Fig. 1a). The central position (X) of a particular cargo was obtained from fluorescence images (Methods), and anterograde transport was set to the plus X direction. Fig. 1b shows typical example trajectories of the positions, in which cargo velocities for anterograde (Fig.1b, top) and retrograde (Fig. 1b, bottom) transport changed over the course of several seconds. In particular, the constant velocity segments (CVSs) of the trajectories (Fig.1b, grey arrows) were focused for the following analyses, assuming that CVS fluctuation (seen in Fig. 2a) in one direction was minimally affected by other motors (Supplementary Fig. S1 for more detailed information).

The fluctuation property of a CVS is represented by the distribution $P(\Delta X)$ (Fig. 2b), where $\Delta X = X(t + \Delta t) - X(\mathrm{t})$ (Fig. 2a). $P(\Delta X)$ for one CVS, as well as those obtained for other cargo [6, 7, 8], was well described by a Gaussian function. The diffusion coefficient (D) of a moving cargo at a CVS was then calculated from the variance (σ^2) of $P(\Delta X)$ using the

equation $\sigma^2 = 2D\Delta t$. Note that the abnormal diffusion property [i.e., $P(\Delta X)$ is not a Gaussian function] often reported for intercellular cargo transport[9, 10] appeared upon analysis of an entire whole trajectory without dividing it into CVSs[11]. One reason for the abnormality in D might be that the trajectory includes multiple velocity values.

D for a moving cargo at a CVS as a function of Δt became constant for large Δt (Fig. 2c). The relaxation time (~20 ms) demonstrated in Fig. 2c is considered the characteristic time of microscopic interactions, such as tethering interactions between the cargo and microtubules, collisions with other organelles and cytoskeletons, and ATP hydrolysis by motors[7]. For diffusion of a cargo on a large time scale (Δt ~100 ms) (Fig. 2c), such microscopic interactions are thought to act on the cargo as effective viscosity (η_{eff}), as well as the viscosity of the cytosol[7]. The convergent value of D was then plotted as a function of fluorescence intensity (FI) of the cargo (Fig. 2d), where FI is proportional to the surface area of the cargo $\propto r^2$ (r: cargo radius). For smaller vesicles ($\mathrm{FI} < 1000\,\mathrm{a.u.}$), D exhibits Einstein relation-like behavior ($D \propto \mathrm{FI}^{-1/2} \propto 1/r \propto 1/\Gamma$), where $\Gamma\,(= 6\pi\eta_{\mathrm{eff}}\mathrm{r})$ represents the friction coefficient of a cargo. For larger vesicles ($\mathrm{FI} > 1000\,\mathrm{a.u.}$), D decreases more sharply ($\propto \mathrm{FI}^{-1}$), indicating that η_{eff} becomes dependent on r. Such size-dependent effective viscosity was previously reported for beads (>150 nm) incorporated in cells affected by intracellular complex structures[11].

Velocities of CVSs of moving cargos

We next investigated the anterograde and retrograde velocities of CVSs (Fig. 2e–g), finding mean values of 1.3 μm/s and 0.94 μm/s, respectively, for each type of transport. We used the absolute values for velocity in order to allow representation of the retrograde velocity as a positive value. The mean values were smaller to those obtained for other axonal cargo transport measured via kymograph analysis[12], possibly because smaller, fast-moving vesicles could not be tracked by our particle tracking software.

The velocity values were widely distributed (100 nm/s < $v \leq 3$ μm/s) (Fig. 2e) and decreased along with increases in FI (Fig. 2f); however, the correlation between velocity and FI ($R = -0.33$, $p=4\times10^{-7}$) was weaker than that between D and FI ($R = -0.47$, $p=7\times10^{-6}$) (Fig. 2d),

potentially indicating a dependence of v on another quantity, such as the number of force producing units (FPUs) carrying a cargo comprising the motor proteins (Fig.1a, bottom), as well as cargo size. This dependence of v on the number of FPUs is explained by the force–velocity model described in Fig. 2h and was previously suggested for kinesin to interpret *in vitro* single-molecule experiments applying loads to kinesin using optical tweezers[13]; however, force–velocity relationships for dynein have not been clarified. The stall force (F_s) (Fig. 2h), which is the maximum force that kinesin can exert, is proportional to the number of FPUs. Additionally, the line in Fig. 2h illustrates the Stokes relation $v = F/\Gamma$ for a cargo in motion. The intersections of the force–velocity curves and Stokes relation provide the measured velocities of the cargo in cases of one, two, and three FPUs, respectively. According to the model (Fig. 2h), the velocity values can be changed (e.g., v_1, v_2, and v_3) as the number of FPUs changes under high load (viscosity) conditions. Therefore, the velocity changes observed in Fig. 1b were considered to occur as a result of changes in the number of FPUs, which would agree with previously reported changes in experimental velocity[8, 14].

To determine whether the high load condition that the mean velocity ($\langle v \rangle$) was markedly smaller than the maximum velocity $v_{\max}$ during anterograde transport (Fig. 2h), we estimated $v_{\max}$ using extreme-value statistics. Note that $v_{\max}$, regarded as the anterograde velocity with no load, could not be measured directly in the axons, because kinesin without cargo (representing load to the kinesin) exists in an autoinhibited state in cells[15]. First, for an anterograde trajectory during 20 s of movement of the i-th cargo, $v_{\max}^i$ was defined as the measured maximum velocity of the i-th cargo that appeared during the period. For 188 anterograde cargos investigated, we plotted the cumulative distribution (G) of $\{v_{\max}^i\}$ (Fig. 2g) as the second procedure, and fit G using extreme-value statistics[16] according to the function

$$G\left(v_{\max}^i; \mu, \sigma, \xi\right) = \exp\left\{-\left[1 + \xi\left(\frac{v_{\max}^i - \mu}{\sigma}\right)\right]^{-1/\xi}\right\} \qquad (1)$$

where $\mu, \sigma,$ and ξ are fitting parameters. We found $\xi < 0$ and obtained the maximum value of 5.8±0.23 μm/s as $\mu - \sigma/\xi$ (see Fig. S2 for results from other datasets). We then compared the mean $\langle v \rangle$ and maximum $v_{\max}$ velocities (Fig. 2i), finding that $\langle v \rangle \ll v_{\max}$ and indicating realization of the high load condition for anterograde transport. In subsequent paragraphs, we assumed the high load condition for the case of retrograde transport because

the force–velocity relationship for dynein was unknown.

Force index (χ) and the number of FPUs transporting a cargo

The comparison between $\langle v \rangle$ and $v_{\max}$ (Fig. 2i) showed that the load acting on a cargo was considered large enough that the value of drag force (Γv) was close to the stall-force value (F_s). Because the stall-force value is proportional to the number (n) of FPUs, it is considered to approximate $\Gamma v \propto n$ when the load on a cargo is large enough. As a substitute for the unknown value of $\Gamma (= 6\pi\eta_{\mathrm{eff}} r)$, when we use D^{-1} [assuming that $D \propto 1/\Gamma$], we define a force index (χ) as follows:

$$\chi(\Delta t) \equiv \frac{v}{D(\Delta t)} \qquad (2)$$

This is expected to have the approximated relationship: $\chi \propto n$. χ was first introduced to investigate endosome transport in mouse dorsal root ganglion neurons[7] and extended to synaptic vesicle precursor transport in the motor neurons of *Caenorhabditis elegans* [6] and melanosome transport in zebrafish melanophores[8] in order to count the number of FPUs. In these previous studies, χ was turned out to be quantal and reflect the number of FPUs. Here, we noted that F and F_s could not be directly measured in the axons using optical tweezers based on the small size of the synaptic cargos (~100 nm) and the difficulty in force calibration of the optical tweezers in the complex intracellular environment. Therefore, we used χ [Eq. (2)], which was non-invasively measured unlike F_s measured using optical tweezers, to obtain force information.

We plotted the force index, χ, as a function of Δt for anterograde and retrograde transport, respectively (Fig. 3). χ converged after a period of time due to the Δt-dependence of D (Fig. 2c), whereas v was almost constant for all Δt. When the discreteness of χ represented the discreteness of transport force, we identified seven FPUs used for anterograde transport and five FPUs for retrograde transport. Additional FPUs were needed for anterograde transport possibly because one FPU of kinesin comprises a dimer, whereas that of dynein comprises four dynein monomers according to cryo-electron microscopy[17].

Addition of the dynein inhibitor

Finally, we investigated the effect of the drug ciliobrevin[18] that inhibits ATPase activity of AAA+ ATPase superfamily proteins, including dynein. We treated the cells with ciliobrevin during 30 min in order to measure the effect on FPU number and plotted outcomes in the presence of 200 μM and 500 μM ciliobrevin for anterograde (Fig. 3b,c) and retrograde (Fig. 3e,f) transport, respectively. Although changes in anterograde FPUs were small (Fig. 3b,c), retrograde FPUs showed larger decreases in the presence of higher concentrations of ciliobrevin (Fig. 3e,f). Because ciliobrevin inhibits dynein, this result confirmed a lack of effect on kinesin-specific cargo transport.

We then measured the effect of ciliobrevin on other physical parameters, including run time and velocity (Fig. 4), because these quantities also depend on the number of FPUs carrying cargo. We found that the run time of a moving cargo was defined as the duration between pauses, with a pause defined as a duration >0.25 s at a velocity <100 nm/s (Fig. 4a). The run time is dependent on the number of FPUs, because cargo transported by multiple FPUs seldom detaches from microtubules, thereby making the run time longer. Fig. 4b shows histograms of the run times for anterograde (left) and retrograde (right) transport. As ciliobrevin concentration increased, we observed a more obvious decrease in retrograde transport, confirming that similar behavior as that observed for χ measurements (Fig. 3) and velocity at CVSs (Fig. 4c).

After quantifying the number of FPUs, run time, and velocity for moving cargos, we then evaluated changes in the amount of moving cargos over a period of 20 s in an area of 22 μm × 22 μm (Fig. 4d, left) as a function of ciliobrevin concentration (Fig. 4d, right). We observed that the number of moving cargos rapidly decreased bidirectionally. Similar bidirectional damages caused by inhibitors of motors have been reported for several types of cargo transport, suggesting that anterograde and retrograde transport are closely linked through a common regulatory mechanism[19, 20, 21]. We found that such a regulation did not involve only the inactivation of kinesin in the case of ciliobrevin, as the change in anterograde FPUs was small (Fig. 3b-c).

Summary

In summary, in this study, we used extreme-value statistics (Fig. 2g, Supplementary Fig. S2)

and non-invasive force measurement using χ [Eq. (2)] (Fig. 3) to estimate the physical parameters associated with intracellular transport, and quantified the effect of the dynein inhibitor ciliobrevin on cargo transport. Given the difficulty of direct physical measurement in cells, we hope that application of these techniques promotes further understanding of the mechanisms of intracellular cargo transport through statistical estimation of the associated parameters.

Methods

Primary culture of neurons and transfection

Primary culture of hippocampal neurons was performed using a modified version of a previously described method[12, 22]. The hippocampus of wild-type C57BL/6 mice (Japan SLC, Hamamatsu, Japan) at embryonic day 17 was dissected, and neurons were cultured in glass-bottom dishes (MatTek, Ashland, MA, USA) with the culture medium (NbActiv4; BrainBits, Springfield, USA), as described previously[12]. After culture for 4 to 7 days, neurons were transfected with the plasmids vector for GFP-fused synaptotagmin[23] using the calcium phosphate method (Takara Bio, CA, USA). All animal experiments were conducted in compliance with a protocol approved by the Institutional Animal Care and Use Committee, Tohoku University.

Ciliobrevin treatment and fluorescence observation of synaptic cargos

Ciliobrevin D (Merck, Kenilworth, NJ, USA) was added to a culture dish with neurons and incubated for 30 min prior to fluorescence observation. The final ciliobrevin concentration was determined to be less than 1 mM, based on the lack of mobile SVPs observed during 30-min treatment with 1 mM ciliobrevin.

At 1-day post-transfection, neurons were washed twice with phenol red-free Hank's balanced salt solution (Thermo Fisher Scientific, Waltham, MA, USA) and observed with a fluorescence microscope (IX83; Olympus, Tokyo, Japan) equipped with a heating plate (CU-201; Live Cell Instrument, Seoul, Korea) maintained at 37 °C. For this observation, B27-supplement (Thermo Fisher Scientific) and 150 μM 2-Mercaptoethanol (Wako Chemical Co., Tokyo, Japan) were added to Phenol Red-free Hank's balanced salt solution. Images of motile cargo was obtained with a 150× objective lens (UApoN 150×/1.45; Olympus) and an sCMOS camera (OLCA-Flash4.0 v.2.0; Hamamastu Photonics, Hamamatsu, Japan) at 100 frames/s. The center position of each cargo was determined from the recorded image using custom-made software written in LabVIEW 2013 (National Instruments, Austin, TX, USA), as described previously[6].

Totally, the primary culture of neurons was repeated 9 times, and data were collected from five to six preparations of each ciliobrevin concentration. To examine anterograde and

retrograde transport, investigated 137 and 162 cargos from 50 and 39 different cells (0 μM ciliobrevin), 118 and 116 cargos from 34 and 27 different cells (200 μM ciliobrevin), and 99 cargos from 28 and 20 different cells (500 μM ciliobrevin), respectively. The cells used for observation were chosen randomly after visual inspection. The accuracy of the positional measurement was verified with beads (300-nm latex beads; Polyscience, Niles, IL, USA). The standard deviation of the position of the bead tightly attached to the glass surface was 8.3 ± 1.2 nm (n = 4 different beads).

Calculation of χ

The force index χ introduced in our previous studies[6, 7, 8] was originally defined using the idea of the fluctuation theorem as follows:

$$\chi = \ln[\mathrm{P}(\Delta X)/\mathrm{P}(-\Delta X)]/\Delta X \qquad \text{(M1)}$$

from the distribution $P(\Delta X)$ of the displacement $\Delta X = X(t + \Delta t) - X(t)$ (Fig. 2a). $P(\Delta X)$ was fitted with a Gaussian function:

$$P(\Delta X) = \exp(-(\Delta X - b)^2/2a)/(2\pi a)^{0.5} \qquad \text{(M2)}$$

where the fitting parameters a and b correspond to the variance and mean of the distribution, respectively. By inserting Eq. (M2) into Eq. (M1), we obtain:

$$\chi = 2b/a \qquad \text{(M3)}$$

which is equal to Eq. (2). The error of χ was estimated at 10% based on the boot-strapping method[6, 8].

A smoothing filter was applied to the values of χ to reduce variation in the raw data for χ as a function of Δt. We used the following simple averaging filter:

$$\chi^{\mathrm{f}}(\Delta t) = (\chi(\Delta t - 10\mathrm{ms}) + \chi(\Delta t) + \chi(\Delta t + 10\mathrm{ms}))/3 \qquad \text{(M4)}$$

Note that $\chi^{\mathrm{f}}(\Delta t) = (\chi(\Delta t) + \chi(\Delta t + 10\mathrm{ms}))/2$ for $\Delta t = 10\mathrm{ms}$ and $\chi^{\mathrm{f}}(\Delta t) = (\chi(\Delta t - 10\mathrm{ms}) + \chi(\Delta t))/2$ for $\Delta t = 100\mathrm{ms}$. The software used to calculate χ is available from a website[24].

Classification of χ-Δt plots

The χ-Δt plots ($\{\chi_i^{\mathrm{f}}(\Delta t)\}$ for i=1, ,…, N where N is the number of samples) (Fig. 3) were classified statistically using a modified k-means clustering method. For a given k (the number of clusters), an appropriate initial dataset $\chi_{\mathrm{cc}}^m(\Delta t)$ (m=1,…,k) was used as cluster centers, with the i-th data $\chi_i^{\mathrm{f}}(\Delta t)$ belonging to cluster $m(i) = m$ according to the condition $\min_m \sum_{\Delta t}\left(\chi_i^{\mathrm{f}}(\Delta t) - \chi_{\mathrm{cc}}^m(\Delta t)\right)^2$. $\chi_{\mathrm{cc}}^m(\Delta t)$ was then re-calculated as the average of $\chi_i^{\mathrm{f}}(\Delta t)$,

which belongs to the m-th cluster. This procedure was repeated several times until the clusters were fixed. The final cluster centers were fitted by the curves $a_m(1-e^{-b_m x})+c_m$, where $a_m, b_m,$ and c_m are fitting parameters. Akaike's information criterion (AIC) for the χ-Δt plots was calculated as $N\log[\mathrm{RSS}/\mathrm{N}]+6k$, and $\mathrm{RSS}=\sum_{i=1}^{N}\left[\chi_i^{\mathrm{f}}(\Delta t)-\left(a_{m(i)}\left(1-e^{-b_{m(i)}x}\right)+c_{m(i)}\right)\right]^2$. In the case of the anterograde χ-Δt plots (Fig. 3a), AIC values were −405 for k = 4, −436 for k = 5, −457 for k = 6, −460 for k = 7, and −458 for k = 8. In the case of the retrograde χ-Δt plots (Fig. 3d), AIC values were −341 for k = 3, −394 for k = 4, −413.0 for k = 5, −422 for k = 6, and −233 for k = 7. From these AIC values and the classification results obtained for previous experiments on axonal transport [6, 7], the most probable values of k were determined as k =7 for anterograde (Fig. 3a) and k = 5 for retrograde (Fig. 3d) transport.

Statistics

For the dataset (x_i, y_i) in Fig. 2d,f, the correlation coefficient was calculated using the following equation

$$R=\frac{\sum_{i=1}^{N}(x_i-\langle x\rangle)(y_i-\langle y\rangle)}{\sqrt{\sum_{i=1}^{N}(x_i-\langle x\rangle)^2}\sqrt{\sum_{i=1}^{N}(y_i-\langle y\rangle)^2}} \tag{M5}$$

The p-value was calculated by using the cor.test program of the R software[25].

Acknowledgements

We acknowledge Dr. K. Chiba for providing the method used to culture hippocampal neurons and S. Hasegawa for help with the particle-tracking software. We would like to thank Editage (www.editage.com) for English language editing. This work was supported by JST PRESTO (grant No. JPMJPR1877), AMED PRIME (grant No. JP18gm5810009), and JSPS KAKENHI (grant No. 17H03659) to K. H., as well as JSPS KAKENHI (grant Nos. 17H05010 and 19H04738) to S. N.

Author Contributions

K.H. and M.G.M performed the experiments. K.H. analyzed the data and wrote the paper with contributions from S.N.

Competing Interests: The authors declare no competing interests.

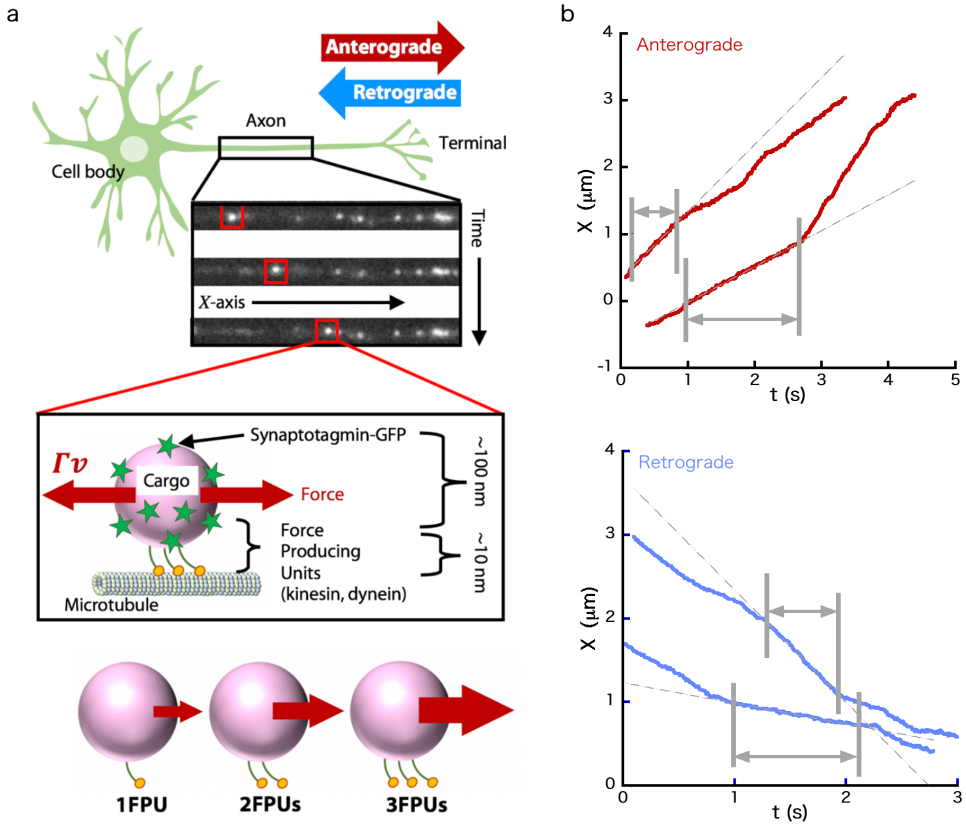

Fig. 1 Synaptic protein transport in the axon of a hippocampal neuron. (a) Schematic of transport. Synaptic cargos undergo anterograde transport by kinesin and retrograde transport by dynein along microtubules. White dots in the micrographs represent synaptic cargos. Although the axons were crowded with cargos, we were able to track some individual cargos. The force is generated by the motor proteins and equivalent to the drag force, Γv, at a constant velocity segment (CVS), where v and Γ represent the velocity and friction coefficient of a cargo, respectively. A single cargo transported by multiple force producing units (FPUs) comprising the motor proteins (bottom). Under high load conditions, the increase of force exerted by motors represent the increase of FPUs. (b) Typical examples of time courses of cargo positions (X) during anterograde (top) and retrograde (bottom) transport, respectively. The time intervals (grey arrows) represent CVSs.

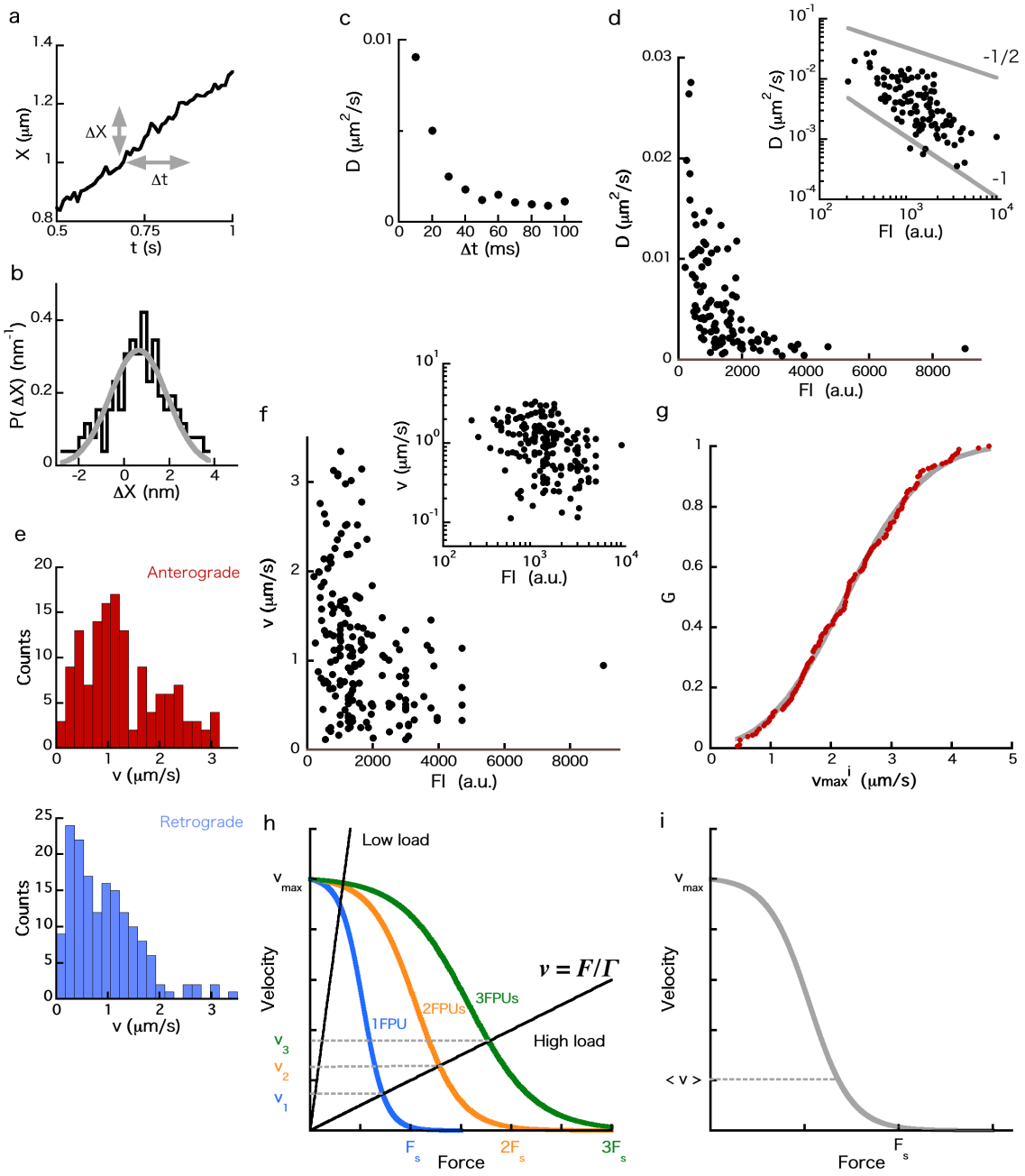

Fig. 2 Fluctuation property and velocity of synaptic cargo transport. (a) Magnified view of the time course (Fig. 1b) in a CVS. $\Delta X = X(t + \Delta t) - X(t)$. (b) Distribution of ΔX for Δt =10 ms. $P(\Delta X)$ was fitted well by a Gaussian function with variance $\sigma^2 (= 2D\Delta t)$ (c) Example of D for a moving cargo at a CVS. (d) The convergent value of D plotted as a function of fluorescence intensity (FI) of a cargo. 108 cargos were investigated. Here, data for anterograde and retrograde transport were not separated. The inset represents the logarithmic expression, and grey lines represent $FI^{-1/2}$ and FI^{-1}, respectively. (e) Histograms for velocity at

a CVS for anterograde (top) and retrograde (bottom) transport. (f) Velocity at a CVS is plotted as a function of FI. 182 cargos were investigated. The inset represents the logarithmic expression. (g) Extreme-value statistics analysis of velocity. The cumulative function (G) for anterograde transport. The fitted function (grey) represents Eq. (1) with the parameters $\mu = 1902 \pm 5$(SE) μm/s, $\sigma = 985 \pm 9$(SE) μm/s, and $\xi = -0.254 \pm 0.015$(SE). (h) Force–velocity relation model of kinesin. Each colour represents the case of one (blue), two (orange), and three (green) FPUs, respectively. $v = F/\Gamma$ represents the Stokes relation, where Γ is the friction coefficient of a cargo, F is the force acting on the cargo (Fig. 1a), and F_s is the stall force of a kinesin. (i) Comparison of the mean velocity $\langle v \rangle$ and $v_{\max}$ indicating the high load condition depicted in (h).

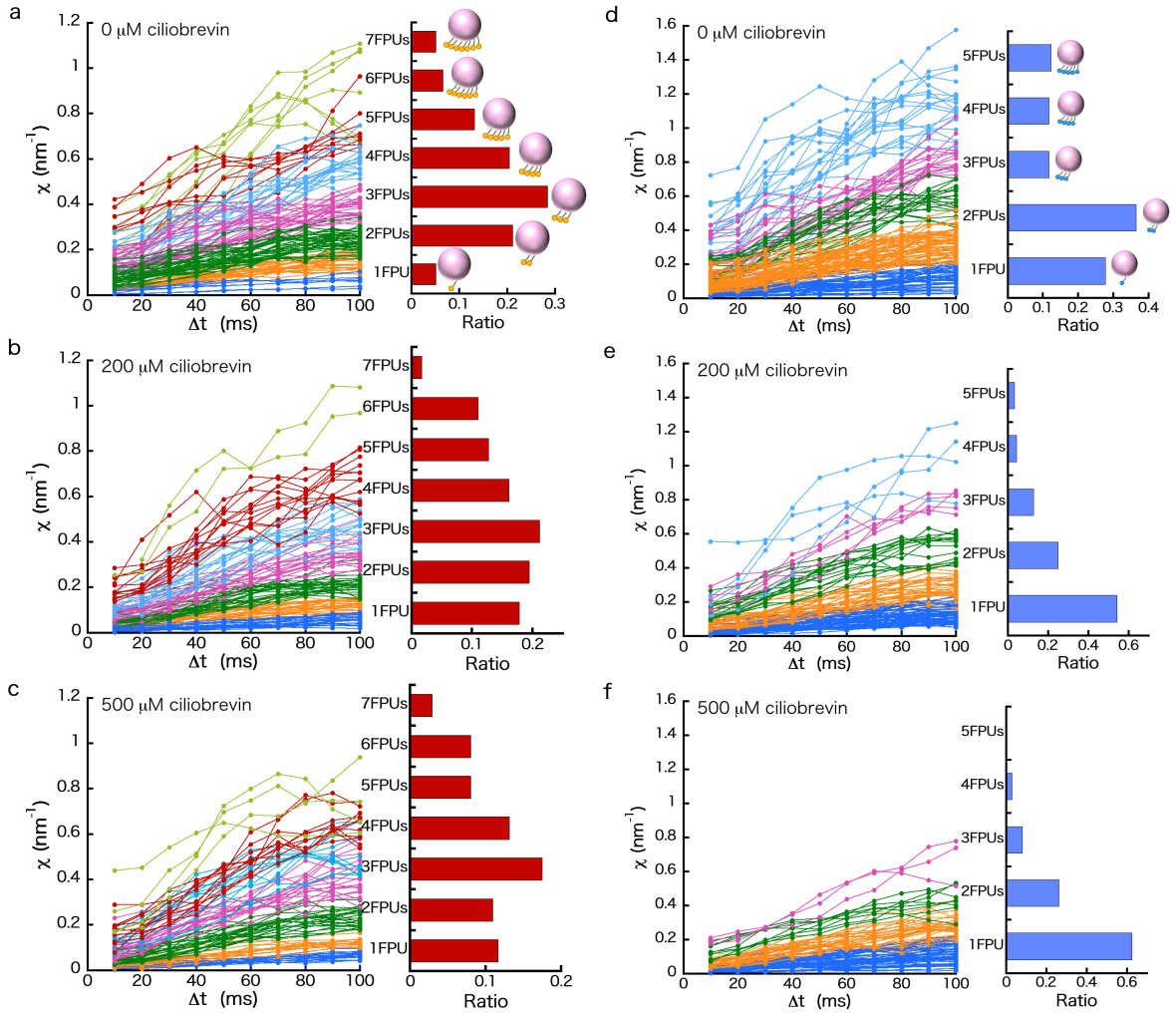

Fig. 3 Force index χ for anterograde (a-c) and retrograde (d-f) transport. χ as a function of Δt for about 100 different cargos in the cases of (a,d) 0 μM, (b,e) 200 μM, and (c,f) 500 μM ciliobrevin (left panels). Each colour denotes each FPU (1, blue; 2, orange; 3, green; 4, pink; 5, aqua, 6, red; and 7, yellow-green). Data were classified using *k*-means clustering and evaluated by AIC (Methods). The right panels represent FPU ratios.

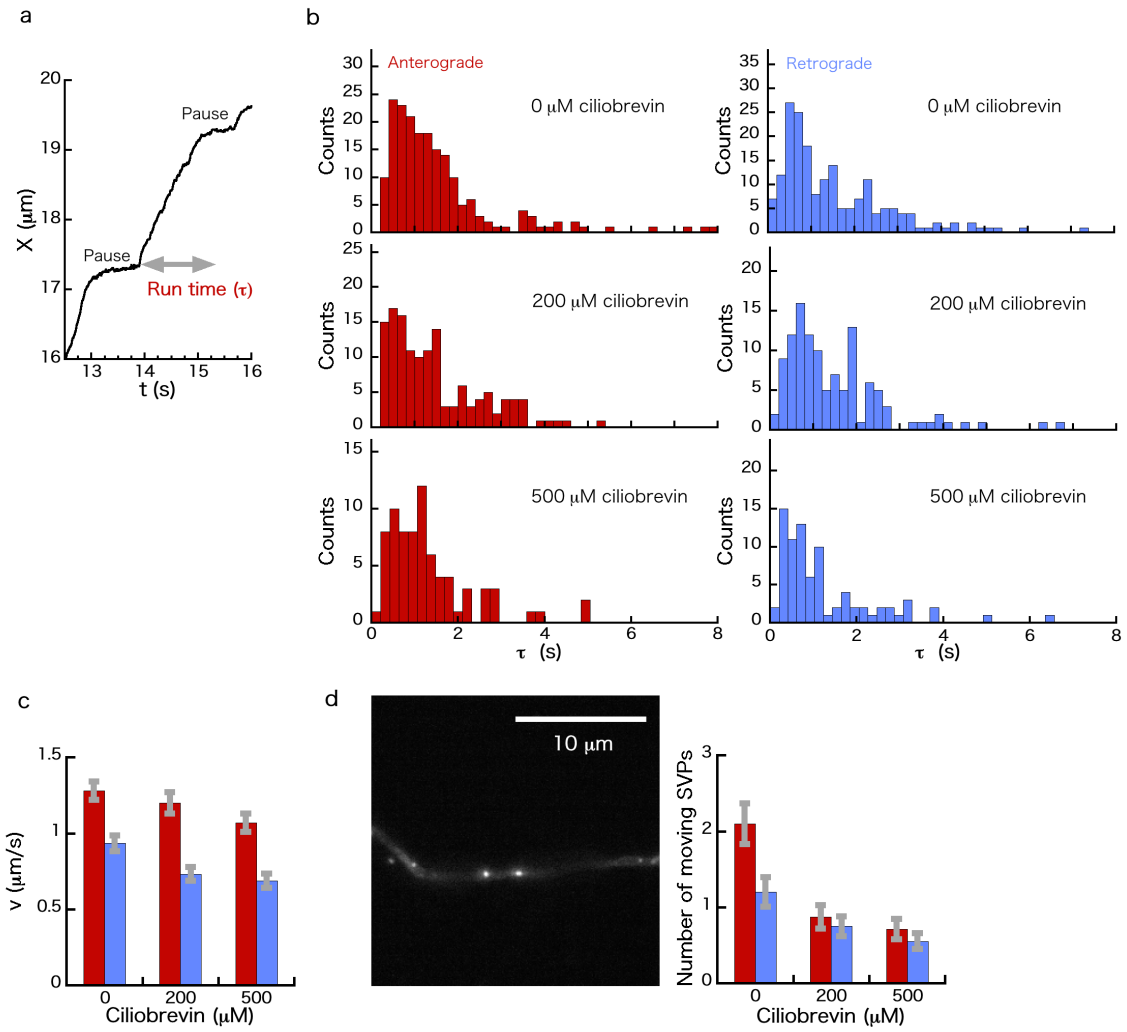

Fig. 4 Effect of ciliobrevin on parameters related to synaptic cargo transport. (a) Definition of run time (τ) (grey arrow) and (b) run-time distributions for anterograde (left) and retrograde (right) transport in the presence of 0 μM (top), 200 μM (middle), and 500 μM (bottom) ciliobrevin. (c) Mean velocities of cargos at CVSs as a function of ciliobrevin concentration. (d) Moving cargos within a 22 um × 22 um area over a 20 s time period (left) as a function of ciliobrevin concentration (right). All error bars represent the standard error.

Reference

1. Hirokawa N, Noda Y, Tanaka Y, Niwa S. Kinesin superfamily motor proteins and intracellular transport. *Nat Rev Mol Cell Biol* 2009, **10**(10)**:** 682-696.

2. Vale RD. The molecular motor toolbox for intracellular transport. *Cell* 2003, **112**(4)**:** 467-480.

3. Guedes-Dias P, Holzbaur ELF. Axonal transport: Driving synaptic function. *Science* 2019, **366**(6462).

4. Encalada SE, Goldstein LS. Biophysical challenges to axonal transport: motor-cargo deficiencies and neurodegeneration. *Annu Rev Biophys* 2014, **43:** 141-169.

5. Gabrych DR, Lau VZ, Niwa S, Silverman MA. Going Too Far Is the Same as Falling Short(dagger): Kinesin-3 Family Members in Hereditary Spastic Paraplegia. *Front Cell Neurosci* 2019, **13:** 419.

6. Hayashi K, Hasegawa S, Sagawa T, Tasaki S, Niwa S. Non-invasive force measurement reveals the number of active kinesins on a synaptic vesicle precursor in axonal transport regulated by ARL-8. *Phys Chem Chem Phys* 2018, **20**(5)**:** 3403-3410.

7. Hayashi K, Tsuchizawa Y, Iwaki M, Okada Y. Application of the fluctuation theorem for non-invasive force measurement in living neuronal axons. *Mol Biol Cell* 2018**:** mbcE18010022.

8. Hasegawa S, Sagawa T, Ikeda K, Okada Y, Hayashi K. Investigation of multiple-dynein transport of melanosomes by non-invasive force measurement using fluctuation unit chi. *Sci Rep* 2019, **9**(1)**:** 5099.

9. Fakhri N, Wessel AD, Willms C, Pasquali M, Klopfenstein DR, MacKintosh FC*, et al.* High-resolution mapping of intracellular fluctuations using carbon nanotubes. *Science* 2014, **344**(6187)**:** 1031-1035.

10. Shin K, Song S, Song YH, Hahn S, Kim JH, Lee G*, et al.* Anomalous Dynamics of in

Vivo Cargo Delivery by Motor Protein Multiplexes. *J Phys Chem Lett* 2019, **10**(11)**:** 3071-3079.

11. Hayashi K, Pack CG, Sato MK, Mouri K, Kaizu K, Takahashi K*, et al.* Viscosity and drag force involved in organelle transport: investigation of the fluctuation dissipation theorem. *Eur Phys J E Soft Matter* 2013, **36**(12)**:** 136.

12. Chiba K, Araseki M, Nozawa K, Furukori K, Araki Y, Matsushima T*, et al.* Quantitative analysis of APP axonal transport in neurons: role of JIP1 in enhanced APP anterograde transport. *Mol Biol Cell* 2014, **25**(22)**:** 3569-3580.

13. Schnitzer MJ, Visscher K, Block SM. Force production by single kinesin motors. *Nat Cell Biol* 2000, **2**(10)**:** 718-723.

14. Hayashi K, Matsumoto S, Miyamoto MG, Niwa S. Physical parameters describing neuronal cargo transport by kinesin UNC-104. *Biophys Rev* 2019, **11**(3)**:** 471-482.

15. Niwa S, Lipton DM, Morikawa M, Zhao C, Hirokawa N, Lu H*, et al.* Autoinhibition of a Neuronal Kinesin UNC-104/KIF1A Regulates the Size and Density of Synapses. *Cell Rep* 2016, **16**(8)**:** 2129-2141.

16. Takahashi R, Shimura T. *Extreme Vale Statistics*. Kindai-Kagaku-Sha: Tokyo, 2016.

17. Urnavicius L, Lau CK, Elshenawy MM, Morales-Rios E, Motz C, Yildiz A*, et al.* Cryo-EM shows how dynactin recruits two dyneins for faster movement. *Nature* 2018, **554**(7691)**:** 202-206.

18. Firestone AJ, Weinger JS, Maldonado M, Barlan K, Langston LD, O'Donnell M*, et al.* Small-molecule inhibitors of the AAA+ ATPase motor cytoplasmic dynein. *Nature* 2012, **484**(7392)**:** 125-129.

19. Waterman-Storer CM, Karki SB, Kuznetsov SA, Tabb JS, Weiss DG, Langford GM*, et al.* The interaction between cytoplasmic dynein and dynactin is required for fast axonal transport. *Proc Natl Acad Sci U S A* 1997, **94**(22)**:** 12180-12185.

20. Brady ST, Pfister KK, Bloom GS. A monoclonal antibody against kinesin inhibits both anterograde and retrograde fast axonal transport in squid axoplasm. *Proc Natl Acad Sci U S A* 1990, **87**(3)**:** 1061-1065.

21. Sainath R, Gallo G. The dynein inhibitor Ciliobrevin D inhibits the bidirectional transport of organelles along sensory axons and impairs NGF-mediated regulation of growth cones and axon branches. *Dev Neurobiol* 2015, **75**(7)**:** 757-777.

22. Bartlett WP, Banker GA. An electron microscopic study of the development of axons and dendrites by hippocampal neurons in culture. I. Cells which develop without intercellular contacts. *J Neurosci* 1984, **4**(8)**:** 1944-1953.

23. Niwa S, Takahashi H, Hirokawa N. beta-Tubulin mutations that cause severe neuropathies disrupt axonal transport. *EMBO J* 2013, **32**(10)**:** 1352-1364.

24. It'll be provided via GitHub.

25. R Core Team (2018). R: A language and environment for statistical computing. R Foundation for Statistical Computing, Vienna, Austria. URL https://www.R-project.org/.

Supplementary Information

Supplementary Figures S1-S2

Physical parameters characterizing dysfunction of neuronal cargo transport caused by the dynein inhibitor ciliobrevin

Kumiko Hayashi, Miki G. Miyamoto, and Shinsuke Niwa

Supplementary Figure S1

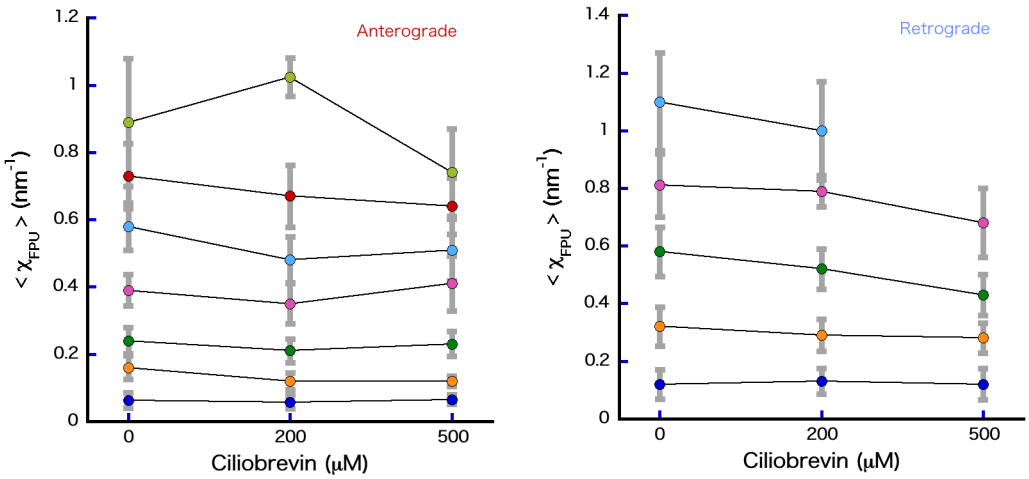

Fig. S1 Mean values of χ (Δt=100 ms) for each FPU as a function of ciliobrevin concentration in the cases of anterograde (left) and retrograde (right) transport. The error-bars represent the standard deviation (SD). Each colour denotes each FPU shown in Fig. 3. In the bidirectional transport system, we assumed that CVS fluctuation (seen in Fig. 2a) in one direction was minimally affected by other motors. This assumption is not trivial, because the tug-of war motion[1, 2, 3] between two motors, which could be an origin of this fluctuation, occurs during changes in direction. Fig. S1 shows the mean value of the force index ($\langle\chi_{\mathrm{FPU}}\rangle$) for each FPU as a function of ciliobrevin concentration. Each anterograde $\langle\chi_{\mathrm{FPU}}\rangle$ showed a small change along with increases in ciliobrevin concentration (Fig. S1, left), indicating that anterograde CVSs used to calculate $\langle\chi_{\mathrm{FPU}}\rangle$ were relatively unaffected by dynein inhibition. This suggested that the tug-of-war motion between kinesin and dynein is unlikely the origin of macroscopic fluctuations in the CVS, given the sensitivity of the tug-of-war motion to the number of dynein monomers.

Supplementary Figure S2

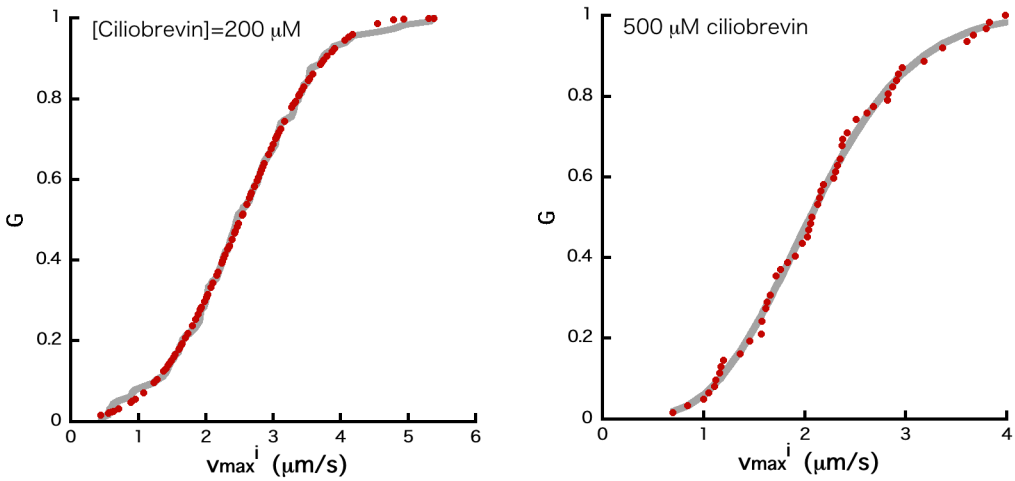

Fig. S2 Extreme-value statistics analysis of anterograde velocity in the cases of 200 μM (left) and 500 μM (light) ciliobrevin. The cumulative functions (G) for anterograde transport were plotted. The fitted functions (grey) represents Eq. (1) with the parameters $\mu = 2173 \pm 4$(SE) μm/s, $\sigma = 973 \pm 8$(SE) μm/s, and $\xi = -0.296 \pm 0.013$(SE) in the case of 200 μM ciliobrevin, and $\mu = 1801 \pm 8$(SE) μm/s, $\sigma = 717 \pm 14$(SE) μm/s, and $\xi = -0.149 \pm 0.029$(SE) in the case of 500 μM ciliobrevin. The maximum velocity was calculated as $\mu - \sigma/\xi$ to be 5.5±0.15 μm/s in the case of 200 μM ciliobrevin, and 6.6±0.94 μm/s in the case of 500 μM ciliobrevin. Note that we converted the estimated value of $v_{\max}$ to ATPase activity (~700 s^{-1}), which was ~3-fold higher than that observed in *in vitro* single-molecule experiments[4]; however, an explanation for the higher ATPase activity under intracellular conditions remains to be clarified

Supplementary References

1. Gross SP. Hither and yon: a review of bi-directional microtubule-based transport. *Phys Biol* 2004, **1**(1-2)**:** R1-11.

2. Welte MA. Bidirectional transport along microtubules. *Curr Biol* 2004, **14**(13)**:** R525-537.

3. Muller MJ, Klumpp S, Lipowsky R. Tug-of-war as a cooperative mechanism for bidirectional cargo transport by molecular motors. *Proc Natl Acad Sci U S A* 2008, **105**(12)**:** 4609-4614.

4. Chiba K, Takahashi H, Chen M, Obinata H, Arai S, Hashimoto K*, et al.* Disease-associated mutations hyperactivate KIF1A motility and anterograde axonal transport of synaptic vesicle precursors. *Proc Natl Acad Sci U S A* 2019, **116**(37)**:** 18429-18434.